

UC Irvine

UC Irvine Previously Published Works

Title

Silica Nanowire Arrays for Diffraction-Based Bioaffinity Sensing

Permalink

<https://escholarship.org/uc/item/8q40q3dm>

Journal

Chemistry - A European Journal, 20(34)

ISSN

0947-6539

Authors

Loget, Gabriel
Corn, Robert M

Publication Date

2014-08-18

DOI

10.1002/chem.201304800

Peer reviewed



Published in final edited form as:

Chemistry. 2014 August 18; 20(34): 10802–10810. doi:10.1002/chem.201304800.

Silica Nanowire Arrays for Diffraction-Based Bioaffinity Sensing

Dr Gabriel Loget* and Prof. Robert M. Corn

Department of Chemistry University of California-Irvine Irvine, CA 92697 USA

Abstract

Arrays of electrodeposited silica nanowires (SiO₂ NWs) have been fabricated over large areas (cm²) on fluoropolymer thin films attached to glass substrates by a combination of photolithography and electrochemically triggered sol-gel nanoscale deposition. Optical and SEM measurements revealed that the SiO₂ NW arrays had an average spacing of 10 micrometers and an average width of 700 nm with a significant grain structure that was a result of the sol-gel deposition process. The optical diffraction properties at 633 nm of the SiO₂ NWs arrays were characterized when placed in contact with solutions using a prism-coupled total internal reflection geometry; quantification of changes in these diffraction properties was applied in various sensing applications. Bulk refractive index sensing using the SiO₂ NWs grating was demonstrated with a refractive index resolution of 1.30×10^{-5} RIU. Toposelectively chemically-modified SiO₂ NW arrays were used for diffraction biosensing measurements of surface binding events, such as the electrostatic adsorption of gold nanoparticles and the bioaffinity adsorption of streptavidin onto a biotin monolayer. Finally, the application of the SiO₂ NWs arrays for practical medical diagnostic applications was demonstrated by monitoring the diffraction of SiO₂ NWs arrays functionalized with a single-stranded DNA aptamer in order to detect human α -thrombin from solutions at sub-pathologic nanomolar concentrations.

Keywords

silica nanowires; sol-gel; electrodeposition; optical diffraction; biosensing

Introduction

Light diffraction created by an optical interaction with periodic structures on surfaces is highly sensitive to the local interfacial properties of the scattering medium. This phenomenon has been used as the sensing principle for a number of simple, inexpensive and label-free detection methods: pH measurements,^[1] metal deposition monitoring^[2] and the detection of volatile organic compounds,^[3] DNA,^[4,5] antibodies,^[6-8] and bacteria.^[9] Gratings formed from arrays of nanowires that exhibit unique optical and electrical properties have expanded the application of metallic and semiconductor gratings to include organic light-emitting diodes,^[10] optical devices,^[11] memristive memories,^[12] capacitors,^[13] mechanical resonators^[14] and sensors.^[15] Metal,^[16] metal oxide^[13] and polymer^[17] nanowire arrays can be fabricated by a variety of methods: focused ion beam

*gabloget@yahoo.fr.

micromachining,^[18] electron beam lithography,^[19] nanoimprint lithography,^[20] superlattice nanowire pattern transfer^[21] and lithographically patterned electrodeposition (LPNE).^[22,23] These nanowire arrays can be used for *in situ* measurements of surface reactions. For example, the optical diffraction from metal nanowires has been recently characterized^[24] and employed for monitoring the electrodeposition of silver on gold.^[2]

An alternative to metal nanowires for diffraction grating sensor applications are silica nanowires (SiO₂ NWs). SiO₂ NWs have recently attracted great attention for applications in photonic devices due to their photoluminescence^[25-28] and subwavelength guiding properties.^[29-31] The processes reported so far for the synthesis of SiO₂ NWs are usually based on vapor-liquid-solid depositions,^[32] oxidation of Si from a liquid alloy,^[33] chemically triggered sol-gel process^[34] and drawing from bulk glass.^[29] A drawback of these techniques is that they lead to the production of nanowire bundles^[32-34] or individual freestanding nanowires,^[29] which cannot be easily adapted to the formation of nanowire arrays for diffraction.

In this article, we report a new technique, based on a modified LPNE^[22,23] process, for the fabrication of SiO₂ NWs arrays with high aspect-ratio and roughness on a polymer layer (Cytop). The SiO₂ NWs are first characterized by optical and electron microscopy. The diffraction of the SiO₂ NWs array is then studied using total internal reflection (TIR) geometry and a 633 nm laser beam. We demonstrate the high sensitivity toward the changes in bulk refractive index using these surfaces and show that surface modification can also be detected by electrostatically adsorbing gold nanoparticles (AuNPs) on the SiO₂ NWs. We then demonstrate the toposelective chemical biomodification of the SiO₂ NWs by fluorescence microscopy and use biotin-modified SiO₂ NWs to monitor the *in situ* binding of streptavidin. Finally, we functionalize the SiO₂ NWs with an ssDNA aptamer for the detection of human α -thrombin at the nanomolar level.

Results and Discussion

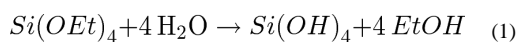
Fabrication of the silica nanowire arrays

The protocol used for the fabrication of the SiO₂ NW arrays on a fluoropolymer film (Cytop) consists of a modified LPNE process that is illustrated in Figure 1.

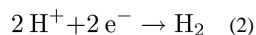
In the classical LPNE process^[22,23] developed by R. M. Penner at UCI, the use of a positive photoresist ((+)PR) is well suited for the electrodeposition of nanowires on glass in an aqueous media; it is not appropriate for the electrodeposition in electrolytes containing ethanol, as the (+)PRs are usually soluble in this solvent. Because sol-gel electrodeposition of silica is usually achieved in a water/ethanol mixture,^[35-38] and since we wanted to fabricate the SiO₂ NWs on substrates other than glass slides, we adapted the LPNE technology to our needs by adding several steps to the process. First, a Cytop film with a thickness of approximately 40 nm was spin-coated on a glass slide (step 1) and a 170 nm-thick nickel layer was then deposited on the Cytop by vapor deposition (step 2). SU-8, an epoxy-based negative photoresist ((-)PR) that is insoluble and resistant to the required solvents was deposited onto the nickel thin film (step 3) and used for patterning stripes with both a width and a spacing of 10 μ m (step 4). A layer of (+)PR was then deposited on the

surface (step 5) and developed (step 6) for protecting the nickel edges from the etching that will be performed in the following step, in order to preserve an electrical conduction pathway between the nickel stripes for the electrodeposition. The nickel was then etched with nitric acid 0.8 M for 14 min (step 7) in order to create nickel stripes with a width smaller than the width of the above (-)PR stripes. This way, two nanotrenches were created at both sides of the nickel stripe between the Cytosol and the (-)PR layer (see inset of step 7). An electrical contact area was then made by dissolving a small part of the (+)PR edge with acetone (step 8).

In sol-gel approaches, a solid phase is formed through gelation of a colloidal suspension (sol).^[39] The sol-gel deposition of SiO₂ coatings on conductive surfaces can be conveniently triggered by electrochemistry.^[35-38] In this approach, a sol is first prepared by hydrolyzing a silica precursor (tetraethyl orthosilicate (TEOS)) in an ethanol/water mixture according to the following reaction (1):



The silica sol is stable at pH 3. Next, a sufficiently negative potential is applied to the working electrode in order to induce proton evolution (2):



The intense pH increase resulting from the consumption of the protons at the electrode surface triggers the polycondensation of the sol.^[35-38] This polycondensation leads to the final SiO₂ coating on the electrode surface. As shown in Figure 1 (step 9), this sol-gel strategy was applied for the electrodeposition of silica onto the nickel confined in the nanotrenches. This was achieved by chronoamperometry at -1.2 V vs Ag/AgCl (NaCl 3M) for 70 s, using the protected nickel substrate as a working electrode. The (+)PR was then dissolved by rinsing the surface with acetone and the (-)PR was removed by immersing the substrate into N-methylpyrrolidinone (NMP) (step 10). Although NMP does not dissolve the (-)PR, it leads to its swelling and its detachment from the substrate over time.^[40] Finally, the remaining nickel was etched (step 11), leading to the formation of the SiO₂ NW array on the Cytosol film.

Characterization of the silica nanowire array

The SiO₂ NWs were characterized by a combination of optical microscopy and scanning electron microscopy (SEM). Figure 2 is a large area view obtained with an optical microscope that shows the SiO₂ NWs array on the Cytosol film.

The SiO₂ NWs can be clearly seen as long and straight clear-colored wires. In this picture, the length of the SiO₂ NWs exceeds 0.5 mm and it was observed that the wires could be fabricated as long as a few millimeters. The wire width is controlled by the electrodeposition time (Figure 1, step 9) and can be estimated from the inset of Figure 2 as 700 nm, which gives, based on the measurements achieved in this figure, an aspect ratio of 750. In reality, this aspect ratio value is much higher because the length of the SiO₂ NWs exceeded the picture frame. The respective spacing between the wires is controlled by two parameters: *i*)

the width of the (-)PR stripes, which is 10 μm (Figure 1, step 4) and *ii*) the nickel etching time, which is 14 min (Figure 1, step 7). The spacing values can be measured from the inset of Figure 2. Because of the nickel etching step, which imparts an asymmetry to the array (Figure 1, step 7), two different values of 9 μm and 11 μm were measured. The smaller value corresponds to the distance between SiO₂ NWs deposited at the two sides of the same nickel stripe and the higher value corresponds to the distance between SiO₂ NWs deposited at the facing sides of two neighboring nickel stripes. As shown in Figure 3, the SiO₂ NWs were further characterized by SEM. Figure 3a shows a section of a single SiO₂ NW, from which a width of 700 \pm 90 nm was measured; this is in good agreement with the previous estimated width value determined by optical microscopy. Figure 3b is a high resolution SEM picture of the surface of a SiO₂ NW, revealing that the SiO₂ surface exhibited a roughness at the nanometer-scale. This important feature can be used advantageously in the context of biosensing by providing a high surface area, which will increase the biosensor sensitivity.

Characterization of the diffraction of the silica nanowire arrays

The diffraction of *p*-polarized visible light at a wavelength of 633 nm by the SiO₂ NW array surface was characterized in water using the optical setup shown in Figure 4a. The glass slide of the SiO₂ NWs substrate was coupled to a glass prism with refractive index matching fluid, positioned onto a rotating stage and the array surface was immersed with water using a flow cell. The incident angle θ on the array surface was positioned beyond the critical angle so that the negative diffraction orders were in total internal reflection (TIR) geometry. The diffraction pattern was projected on a black screen and recorded using a digital camera. The pattern is shown in the top of Figure 4b, the corresponding intensity profile is shown in the bottom part of Figure 4b. The image spot with the largest intensity corresponds to the reflection of the incoming light beam (indicated as 0 order) whereas all the other spots correspond to different orders of diffraction. Among the twelve orders of diffraction shown here, the spot corresponding to the -2 order reveals the highest intensity and therefore was used for the sensing experiments described in the following.

Bulk refractive index sensing using the silica nanowire array diffraction

The sensor characteristics were determined by studying the output signal, *i.e.* the photodiode tension, as a function of the decreasing refractive index n of the solution injected into the flow cell. For these experiments, a photodiode was used to measure the intensity of the $n = -2$ diffraction order. The inset of Figure 5 shows the bulk refractive index detection curve, where the difference of photodiode potential ΔE is plotted as a function of time. The solution at the array surface is successively replaced by pumping five different water/ethylene glycol mixtures of decreasing ethylene glycol (EG) content (%H₂O:%EG = 99:1 to 100:0 (% vol.)), which induces a decreasing of the refractive index n of the light scattering medium (from $n = 1,33279$ RIU to $n = 1,33168$ RIU). Figure 5, which shows ΔE as a function of n , reveals that the intensity of the diffracted spot is directly proportional (linear fit with $R^2 = 0.9873$) to the bulk refractive index of the solution at the array surface. ΔE can thus be employed as the signal transduction for refractive index sensing. From the linear fit of Figure 5, a sensitivity of signal transduction $S = 64.34 \text{ V.RIU}^{-1}$, defined by the slope and a refractive index resolution $R = 1.30 \times 10^{-5}$ RIU, defined by the ratio between the standard deviation and the sensitivity were extracted. This last value is on the same order of

magnitude of the R values reported for most classical surface plasmon resonance (SPR) techniques.^[41,42]

Monitoring of gold nanoparticles electrostatic adsorption

Having shown that changes in the bulk refractive index can be detected using the SiO₂ NW arrays, we demonstrate that the diffraction at the SiO₂ NW arrays can also be used to detect *in situ* surface modifications of the SiO₂ NWs. In a proof-of-principle experiment, we monitored the electrostatic adsorption of a monolayer of negatively-charged AuNPs (with a diameter of ~13 nm, concentration of 8 nM) on the SiO₂ NWs.

The SiO₂ NWs were first modified with amino groups by silanization with (3-aminopropyl)trimethoxysilane (APTMS) in order to generate a positive surface charge. As illustrated in Figure 6a, the modified SiO₂ NWs immersed in water were exposed to negatively-charged AuNPs (citrate-stabilized) and the diffraction changes upon the *in situ* adsorption of the AuNPs onto the silica surface were monitored by diffraction. The adsorption curve is shown in Figure 6b, which shows the photodiode response (ΔE) as a function of time. At 210 s, an aqueous dispersion of AuNPs was injected and an increase in ΔE from 0 to 170 mV was obtained due to the adsorption of AuNPs. Water was re-injected onto the array surface at 910 s which induced a small decrease of the ΔE value to a constant value of 160 mV. This 10 mV decrease is attributed to the detachment of non-electrostatically bound AuNPs, which are removed from the silica surface upon rinsing. This experiment proves that surface modification can be also monitored based on the diffraction at the SiO₂ NW array surface.

Streptavidin adsorption on biotin-modified silica nanowires

In a second set of adsorption measurements, we toposelectively modify the SiO₂ NWs with biotin covalently and use these modified arrays to monitor the bioaffinity adsorption of a streptavidin monolayer. The covalent modification of the SiO₂ NWs with biotin was achieved following a well-known procedure,^[43] which involves first the modification of the silica surface with APTMS, and second the coupling of the amino groups with sulfo-NHS-biotin by the formation of an amide bond. As shown in Figure 7a, the biotin-modified SiO₂ NWs were then exposed to streptavidin. Streptavidin is a tetrameric protein which has four sites for binding biotin^[44] and the biotin-streptavidin bond is one of the strongest known noncovalent interactions, with a dissociation constant in the order of 10⁻¹⁴ M and a reported dissociation half-life of several days.^[45] First, we observed the biotin-modified SiO₂ NWs after their exposure to a solution containing fluorophore-labeled streptavidin (Alexa647) by fluorescence microscopy. The inset of Figure 7b shows the fluorescence picture of the biotin-modified SiO₂ NWs after exposition to the fluorescent streptavidin. In this picture, the SiO₂ NWs are clearly revealed by their fluorescence as 700 nm-wide wires, which corresponds to the previous observations made with the optical microscope as well as at the SEM. As a control experiment, SiO₂ NWs that were not modified with biotin were exposed to fluorescent streptavidin and observed under the fluorescence microscope. No observable fluorescence was detected in this case (as well as at the blank biotin-labeled SiO₂ NW array surface), which proves that no non-specific interaction between the SiO₂ NW and streptavidin is responsible for the fluorescence response at the biotin-modified SiO₂ NW

array surfaces. It can be concluded that streptavidin binds successfully and specifically to the biotin-modified SiO₂ NWs without yielding any non-specific interaction with the underlying Cytosol film.

After having shown that streptavidin specifically binds to biotin-modified SiO₂ NWs, we then demonstrate that it is possible to monitor the *in situ* attachment of streptavidin on biotin using the array diffraction. First, PBS was guided through the flow cell and subsequently a 2.5 μM solution of streptavidin in PBS was injected on the array at 50 s. The detected development of the photodiode potential is shown in Figure 7b. The exposure of the biotin-modified SiO₂ NWs to streptavidin induces an immediate increase of E that reaches its maximum of $E_{\max} = 12$ mV at an incubation time of 200 s. The fact that this E_{\max} value is one order of magnitude lower than the one obtained before for the adsorption of a monolayer of AuNPs is attributed to the fact that the local refractive index change, which is induced by the protein layer, is much lower than the one that was previously obtained by the modification with AuNPs. The exposure of SiO₂ NWs, not modified with biotin to streptavidin provokes just a very slight increase of E to a maximal value of $E_{\max} = 0.6$ mV after an exposure time of 200 s (Figure 7b, grey curve). This value is less than 0.1 % of the E obtained with the biotin-modified SiO₂ NW array, which shows again the very low level of non-specific adsorption of streptavidin onto the SiO₂ NWs.

Detection of thrombin with aptamer-functionalized silica nanowires

The SiO₂ NWs were functionalized with a ssDNA aptamer using the poly(L-glutamic acid) (PGlu) attachment chemistry described recently^[46] and human α-thrombin was detected using the diffraction of the aptamer-modified SiO₂ NWs. Thrombin is a serine protease which catalyzes the conversion of soluble fibrinogen to insoluble fibrin,^[47] and induces physiological and pathological blood coagulation. Whereas a low level of thrombin promotes neuroprotection, it has been reported that thrombin concentrations above 50 nM can cause neuronal degeneration and even cell death.^[48] Because of its implication in major pathologies,^[49,50] it is of first importance to detect thrombin for medical diagnosis. Aptamers are specific dsDNA or ssDNA oligonucleotides that fold into well-defined three-dimensional structures and bind with specific targets.^[51,52] Aptamers are designed for the recognition of a wide range of targets such as proteins, peptides and even cells with high affinity and specificity. The thrombin-binding 15-mer (5'-GGTTGGTGTGGTTGG-3') was one of the first *in vitro* selected ssDNA aptamers targeted towards thrombin^[53,54] and is now one of the most studied aptamers.^[55] This aptamer has been previously used for the detection of thrombin with different techniques such as: colorimetry,^[56] fluorescence,^[57] SPR phase imaging,^[58] electrochemistry^[59,60] and electrochemiluminescence.^[61] Here, we use this aptamer covalently attached to the SiO₂ NWs for the detection of human α-thrombin by diffraction.

The modification of the SiO₂ NWs surface with the thrombin-binding aptamer was performed as shown in Figure 8. The applied PGlu-based surface chemistry has been previously reported by our group,^[46] and has been adapted here to the modification of SiO₂ NWs. First, the surface of the SiO₂ NWs was activated by exposing the array surface to an oxygen plasma for a short time (20 s) in order to increase the number of silanol groups (OH

groups) on the silica surface. It is worth mentioning that no morphological change of the Cytop film was observed after this short plasma etching by SEM. Subsequently amino groups were introduced to the SiO₂ NWs by silanization with APTMS. PGLu, a polymer bearing carboxylate groups was then electrostatically adsorbed onto the positively-charged silica surface. Finally, the SiO₂ NWs were covalently modified with the PGLu backbone as well as the thrombin-binding aptamer by the formation of amide bonds. This was achieved by incubation of a solution of the thrombin-binding aptamer coupled to an amino-terminated linker (ssDNA: 5'-NH₂(CH₂)₆T₁₅GGTTGGTGGTTGG-3') and coupling agents 1-Ethyl-3-[3-dimethylaminopropyl]carbodiimide hydrochloride (EDC) and N-hydroxysulfosuccinimide (sulfo-NHS) in PBS. This step yields a surface of aptamer-modified SiO₂ NWs,^[46] which is the final sensing platform demonstrated in this paper.

The detection of human α -thrombin with the aptamer-modified SiO₂ NWs array surfaces was studied by incubation of the sensing surface with a 30 mM target solution in PBS. As a control, this experiment was also performed with a SiO₂ NW array surface with a T₃₀ ssDNA (5'-NH₂(CH₂)₁₂T₃₀-3') instead of the thrombin-binding aptamer. Figure 9b shows the respective diffraction binding curves and reveals that the thrombin-incubation of the aptamer-modified array surface induces an immediate increase of E which saturates at $E_{\max} = 0.47$ mV after an incubation time of 140 s (Figure 9b, red dotted curve). In contrast, the exposition of the control array to the same concentration of thrombin only leads to an increase of E_{\max} of 0.09 mV (Figure 9b, grey dotted curve). This output signal is more than 5 times smaller than the signal obtained with the aptamer-modified array surface and the increase in signal upon thrombin incubation is in this case attributed to non-specific adsorption of the protein onto the control T₃₀ ssDNA-modified SiO₂ NWs. Figure 9b furthermore shows the fits of the two diffraction binding curves with the kinetic equations (3) and (4) for the adsorption and the desorption processes, respectively (Figure 9b, red and grey solid lines).^[62,63]

$$\Delta E = \frac{k_{on} C_{thr} \Delta E_{max}}{k_{on} C_{thr} + k_{off}} \left[1 - e^{-((k_{on} C_{thr} + k_{off})t)} \right] \quad (3)$$

$$\Delta E = \Delta E_0 e^{(-k_{off}t)} \quad (4)$$

with C_{thr} being the concentration of the injected thrombin, E_{\max} the maximum photodiode potential and E_0 the photodiode potential at the beginning of the desorption. From the fit of the desorption part of the red curve of Figure 9b, the aptamer-thrombin dissociation rate constant, k_{off} was obtained. The association constant k_{on} is obtained from equation (3) using the calculated value for k_{off} . The ratio of these two constants k_{on}/k_{off} yields a Langmuir adsorption coefficient^[62,63] $K_{ads} = 8.2 \times 10^7 \text{ M}^{-1}$, which is very close to previous values of K_{ads} obtained by SPR-based sensing techniques reported in the literature for comparable systems.^[58,64] These diffraction experiments demonstrate that SiO₂ NW arrays can be reliably used for the diffraction detection of target proteins with a detection limit sufficiently low to allow the detection of pathologic concentrations of human α -thrombin, which should be of first importance for future applications in medical diagnosis.

Conclusion

In conclusion, we have reported a new technique based on a modified LPNE process involving the electrochemical sol-gel nanodeposition of silica for the fabrication of arrays of SiO₂ NWs with high aspect-ratio and roughness on a fluoropolymer thin film. We have shown their toposelective chemical modification and demonstrated their capability as a diffraction-based sensor by showing four different examples of detection involving bulk refractive index sensing and sensing of nanoparticle and protein adsorption. In particular, we have shown that SiO₂ NWs functionalized with an ssDNA aptamer can be used for the detection of human α -thrombin below pathologic concentrations (30 nM). This fabrication technique could be employed for designing more complex arrays^[8] that could be used for multiplexed detection. In addition to diffraction-based sensing, we believe that these SiO₂ NWs are promising for potential applications in the areas of photoluminescence^[25-28] and waveguides^[29-31] for microfluidic chips.

Experimental Section

Chemicals and material

All the reagents were used as received. The photoresists: SU-8 5 and S1808 as well as the photoresist developers were purchased from MicroChem. Cytop and the Cytop solvent were obtained from AGC. N-methylpyrrolidinone and ethylene glycol (EG) were purchased from Fischer Scientific. 1-Ethyl-3-[3-dimethylaminopropyl]carbodiimide hydrochloride (EDC), N-hydroxysulfosuccinimide (sulfo-NHS) and sulfo-NHS-biotin were purchased from Thermo Scientific. Acetone was obtained from VWR, ethanol from Gold Shield, hydrochloric acid from J. T. Baker and nitric acid from Macron Chemicals. PBS 10 × was obtained from Affymetrix and diluted by 10 with mQ water prior to utilization. Hellmanex, tetraethyl orthosilicate (TEOS), sodium nitrate, (3-aminopropyl)trimethoxysilane (APTMS) and poly(L-glutamic acid) (PGlu) (MW = 50 000-100 000) were purchased from Sigma Aldrich. The aqueous solutions were prepared using milliQ water. The gold nanoparticles (AuNPs) were synthesized using the well-known Turkevich method. The amino-terminated ssDNA sequences were obtained from IDT. Alexa647-streptavidin was purchased from Molecular Probes and Human α -thrombin was obtained from Haematologic Technologies. The glass slides used for the deposition of Cytop were obtained from Fischer. The nickel pellets used for the thermal evaporation were purchased from Kurt J. Lesker.

Preparation of the silica sol

20 mL of an aqueous solution of 0.1 M NaNO₃ was added to 20 mL of ethanol. Under mechanical stirring and using a pH meter (Oakton Instruments) the pH of the mixture was adjusted to a value of 3 using a solution of 0.1 M HCl. 0.4 mL of TEOS was added to the mixture and the solution was left under stirring for 6 hours for hydrolyzing the TEOS.

Fabrication of the silica nanowire arrays

Glass slides (2.5×2.5 cm) were cleaned by ultrasonication in an aqueous solution of Hellmanex (1 % vol.), rinsed thoroughly with water and ethanol and dried under a N₂ stream. The glass slides were then plasma cleaned under an oxygen plasma (Harrick

PDC-32G) for 4 min. A solution of Cytop in solvent (1/5 (w/w)) was spin-coated on the glass slide and the glass slide was left 1h at 90° on a hot plate and 1h at 180° in the oven in order to evaporate the solvent. A layer of 170 nm of nickel was then deposited by vapor deposition (Denton DV 502-A evaporator) on the Cytop layer. SU-8 5 was spin-coated on the nickel layer, soft-baked on a hot plate and the substrate was left for few hours until it reached room temperature. The SU-8 5 photoresist was patterned with lines having a width of 10 μm and a respective spacing of 10 μm using a mask aligner (Karl Suss MJB-3). The substrate was then post-baked on the hot plate, left for few hours in order to reach room temperature, developed using the SU-8 developer and rinsed under a N_2 stream. S1808 was spin-coated on the Ni/SU-8 layer and the photoresist solvent was evaporated at 90° for 20 min in an oven. The positive photoresist was patterned with the mask aligner and developed (using MF-319 developer) in such a way that the edges of the substrate were covered with the S1808 layer. The substrate was rinsed with water and dried under a N_2 flow. The nickel was etched by leaving the substrate in an aqueous solution of 0.8 M nitric acid for 14 min. After rinsing the surface thoroughly with water and drying it with an N_2 flow, an electrical contact area was made by dissolving a small part of the positive photoresist with acetone using a Q-tip. The substrate was then connected to a potentiostat (PGSTAT12, Autolab) and used as a working electrode for the electrodeposition of silica in an O-ring electrochemical cell. The cell was filled with the silica sol, a platinum foil was used as a counter electrode and the deposition was achieved by chronoamperometry at -1.2 V vs Ag/AgCl (3 M NaCl) for 70 s and rinsed with water. The surface was then rinsed with acetone and immersed for 15 min in N-methylpyrrolidinone which resulted in the dissolution of the positive photoresist and the removal of the negative photoresist. The nickel layer was totally etched away by immersing the substrate in 2.7 M nitric acid solution for 30 min. The substrates were finally rinsed with water and dried by a N_2 flow.

Optical microscopy, fluorescence microscopy and SEM characterization

The SiO_2 NWs were observed using a Zeiss Axioskop 2 optical microscope. For the fluorescence microscopy, the biotin-modified SiO_2 NWs were exposed to a $100\ \mu\text{g mL}^{-1}$ Alexa647-streptavidin solution in PBS for 10 min in a humidity chamber. The surfaces were then rinsed with mQ water and dried with a N_2 flow. The imaging was performed using an inverted microscope (Olympus IX71) with an Andor Neo scientific CMOS (South Windsor) camera. For the SEM characterization, a thin layer of iridium was previously sputtered by ion beam sputter deposition (IBS/e, South Bay Technology) on the surface in order to ensure a good electrical conduction. A Philips XL 30 was used for imaging the nanowires and a FEI Magellan 400 XHR was used for the high magnification pictures.

Diffraction experiments

A flow-cell was positioned on the array surface and the outer surface of the surface was coupled to a glass prism using index matching oil (Cargille). The array was positioned on a rotating stage in order to set the incident angle θ . The light was emitted by a 633 nm HeNe laser (JDSU), *p*-polarized using a polarizer (Newport) and diffracted from the array surface. The buffer was passed through the array surface and the incident angle was set to the critical angle, so that the negative diffraction orders were in total internal reflection (TIR) geometry. For the photograph of Figure 4b, the diffraction pattern was projected on a black screen and

photographed using a Canon EOS 40D camera. In all the other experiments the laser was chopped at a frequency of 1.0 kHz (Stanford Research Instruments SR540) and a photodiode (Hamamatsu) connected to a DSP lock-in amplifier (EG&G model 7220) was placed in front of the diffracted spots, the photodiode potential was recorded by a Labview program. For the intensity profile shown in Figure 4b, the photodiode was moved using a rotating stage in order to screen the intensity of the diffraction spot. For all the other experiments, the photodiode was positioned on the diffracted spot having the highest intensity. After obtaining a stable background signal, the solutions containing a mixture of solvents (Figure 5, inset), gold nanoparticles in water (Figure 6b) or proteins in PBS 1× (Figure 7b and 9b) were injected through the flow cell.

Functionalization of the silica nanowires

For the functionalization of the SiO₂ NWs with amino groups, the array surface was first exposed to a 200 mT oxygen plasma (PDC-32G, Harrick Plasma) for 20 s and exposed for 2 h to a solution of 2 % vol. APTMS in ethanol. The substrate was then rinsed with water and ethanol and dried under a N₂ flow. For the functionalization of the SiO₂ NWs with biotin, the amino-functionalized array was exposed to a solution of sulfo-NHS-biotin 5 mM in PBS for 1 h, rinsed with water and dried under a N₂ flow. For the functionalization of the SiO₂ NWs with ssDNA the amino-functionalized array was exposed to a solution of 3 mg mL⁻¹ PGlu in PBS for 1 h, rinsed with water, dried under a N₂ flow and exposed overnight to a PBS solution containing 75 mM EDC, 15 mM sulfo-NHS and 170 mM amino terminated ssDNA. The substrate was finally rinsed with water and dried on a N₂ stream. For the the functionalization with the thrombin-binding aptamer, the ssDNA sequence 5'-NH₂(CH₂)₆T₁₅GGTTGGTGTGGTTGG-3' was used and for the control experiment of Figure 9b, the ssDNA sequence 5'-NH₂(CH₂)₁₂T₃₀-3' was used.

Acknowledgments

This work was supported by the NIH grant R01-GM059622. The authors thank Dr. Nina Loget-Hüsken and Kyunghye Cho for valuable discussions, Dr. Aaron R. Halpern and Dr. Mana Toma for helping with the optical set-up, Jennifer B. Wood for providing the gold nanoparticles and Professor R. M. Penner for the use of its optical microscope. The Laboratory for Electron and X-ray Instrumentation (LEXI) is also acknowledged for the use of their SEMs.

References

- [1]. Nakajima F, Hirakawa Y, Kaneta T, Imasaka T. *Anal. Chem.* 1999; 71:2262–2265. [PubMed: 21662778]
- [2]. Han Y, Corn RM. *J. Phys. Chem. Lett.* 2011; 2:1601–1606. [PubMed: 21743828]
- [3]. Bailey RC, Hupp JT. *J. Am. Chem. Soc.* 2002; 124:6767–6774. [PubMed: 12047198]
- [4]. Bailey RC, Nam J-M, Mirkin CA, Hupp JT. *J. Am. Chem. Soc.* 2003; 125:13541–13547. [PubMed: 14583051]
- [5]. Sendroiu I, Corn R. *Biointerphases.* 2008; 3:FD23–FD29. [PubMed: 20408697]
- [6]. Tsay YG, Lin CI, Lee J, Gustafson EK, Appelqvist R, Magginiti P, Norton R, Teng N, Charlton D. *Clin. Chem.* 1991; 37:1502–1505. [PubMed: 1893575]
- [7]. Yu F, Tian S, Yao D, Knoll W. *Anal. Chem.* 2004; 76:3530–3535. [PubMed: 15228321]
- [8]. Goh JB, Loo RW, Goh MC. *Sens. Actuat. B-Chem.* 2005; 106:243–248.
- [9]. St. John PM, Davis R, Cady N, Czajka J, Batt CA, Craighead HG. *Anal. Chem.* 1998; 70:1108–1111. [PubMed: 9530002]

- [10]. Kang MG, Guo LJ. *Adv. Mater.* 2007; 19:1391–1396.
- [11]. Schider G, Krenn JR, Gotschy W, Lamprecht B, Ditzbacher H, Leitner A, Aussenegg FR. *J. Appl. Phys.* 2001; 90:3825.
- [12]. Yang JJ, Pickett MD, Li X, Ohlberg DAA, Stewart DR, Williams RS. *Nat. Nanotech.* 2008; 3:429–433.
- [13]. Yan W, Ayvazian T, Kim J, Liu Y, Donavan KC, Xing W, Yang Y, Hemminger JC, Penner RM. *ACS Nano.* 2011; 5:8275–8287. [PubMed: 21942449]
- [14]. Melosh NA, Boukai A, Diana F, Gerardot B, Badolato A, Petroff PM, Heath JR. *Science.* 2003; 300:112–115. [PubMed: 12637672]
- [15]. Penner RM. *Annu. Rev. Anal. Chem.* 2012; 5:461–485.
- [16]. Kulkarni GU, Radha B. *Nanoscale.* 2010; 2:2035–2044. [PubMed: 20945550]
- [17]. Arter JA, Taggart DK, McIntire TM, Penner RM, Weiss GA. *Nano Lett.* 2010; 10:4858–4862. [PubMed: 21038915]
- [18]. Steve R, Robert P. J. *Micromech. Microeng.* 2001; 11:287–300.
- [19]. Grigorescu AE, Hagen CW. *Nanotechnology.* 2009; 20:292001. [PubMed: 19567961]
- [20]. Jung G-Y, Li Z, Wu W, Ganapathiappan S, Li X, Olynick DL, Wang SY, Tong WM, Williams RS. *Langmuir.* 2005; 21:6127–6130. [PubMed: 15982008]
- [21]. Heath JR. *Acc. Chem. Res.* 2008; 41:1609–1617. [PubMed: 18598059]
- [22]. Menke EJ, Thompson MA, L C. Xiang, Yang C, Penner RM. *Nat. Mater.* 2006; 5:914–919. [PubMed: 17057701]
- [23]. Xiang C, Yang Y, Penner RM. *Chem. Commun.* 2009:859–873.
- [24]. Halpern AR, Nishi N, Wen J, Yang F, Xiang C, Penner RM, Corn RM. *Anal. Chem.* 2009; 81:5585–5592. [PubMed: 19537714]
- [25]. Yu DP, Hang QL, Ding Y, Zhang HZ, Bai ZG, Wang JJ, Zou YH, Qian W, Xiong GC, Feng SQ. *Appl. Phys. Lett.* 1998; 73:3076–3078.
- [26]. Shang NG, Vetter U, Gerhards I, Hofsäuss H, Ronning C, Seibt M. *Nanotechnology.* 2006; 17:3215–3218.
- [27]. Pang CL, Cui H, Wang CX. *CrystEngComm.* 2011; 13:4082–4085.
- [28]. Alabi TR, Yuan D, Bucknall D, Das S. *ACS App. Mater. Interfaces.* 2013; 5:8932–8938.
- [29]. Tong L, Gattass RR, Ashcom JB, He S, Lou J, Shen M, Maxwell I, Mazur E. *Nature.* 2003; 426:816–819. [PubMed: 14685232]
- [30]. Tong L, Lou J, Gattass RR, He S, Chen X, Liu, Mazur E. *Nano Lett.* 2005; 5:259–262. [PubMed: 15794607]
- [31]. Tong L, Hu L, Zhang J, Qiu J, Yang Q, Lou J, Shen Y, He J, Ye Z. *Opt. Express.* 2006; 14:82–87. [PubMed: 19503319]
- [32]. Gao L, Ji A, Lu N, Li C, Cao Z. *AIP Adv.* 2012; 2:012187.
- [33]. Zheng B, Wu Y, Yang P, Liu J. *Adv. Mater.* 2002; 14:122–124.
- [34]. Zhang M, Bando Y, Wada K, Kurashima K. *J. Mater. Sci.* 1999; 18:1911–1913.
- [35]. Walcarius A, Sibottier E, Etienne M, Ghanbaja J. *Nat. Mater.* 2007; 6:602–608. [PubMed: 17589513]
- [36]. Qu F, Nasraoui R, Etienne M, Côme YBS, Kuhn A, Lenz J, Gajdzik J, Hempelmann R, Walcarius A. *Electrochem. Commun.* 2011; 13:138–142.
- [37]. Lalo H, Bon-Saint-Côme Y, Plano B, Etienne M, Walcarius A, Kuhn A. *Langmuir.* 2012; 28:2323–2326. [PubMed: 22260622]
- [38]. Loget G, Roche J, Gianessi E, Bouffier L, Kuhn A. *J. Am. Chem. Soc.* 2012; 134:20033–20036. [PubMed: 23186018]
- [39]. Lev O, Wu Z, Bharathi S, Glezer V, Modestov A, Gun J, Rabinovich L, Sampath S. *Chem. Mater.* 1997; 9:2354–2375.
- [40]. Dentinger PM, Clift WM, Goods SH. *Microelectron. Eng.* 2002; 61-62:993–1000.
- [41]. Homola J, Yee SS, Gauglitz G. *Sens. Actuat. B-Chem.* 1999; 54:3–15.
- [42]. Stemmler I, Brecht A, Gauglitz G. *Sens. Actuat. B-Chem.* 1999; 54:98–105.

- [43]. Karnik R, Castelino K, Duan C, Majumdar A. *Nano Lett.* 2006; 6:1735–1740. [PubMed: 16895365]
- [44]. Weber P, Ohlendorf D, Wendoloski J, Salemme F. *Science.* 1989; 243:85–88. [PubMed: 2911722]
- [45]. Green, N. *Michael Methods in Enzymology.* Meir, W.; Edward, AB., editors. Vol. 184. Academic Press; 1990. p. 51-67.
- [46]. Chen Y, Nguyen A, Niu L, Corn RM. *Langmuir.* 2009; 25:5054–5060. [PubMed: 19253965]
- [47]. Bode W, Mayr I, Baumann U, Huber R, Stone SR, Hofsteenge J. *Embo J.* 1989; 8:3467–3475. [PubMed: 2583108]
- [48]. Striggow F, Riek M, Breder J, Henrich-Noack P, Reymann KG, Reiser G. *Proc. Natl. Acad. Sci. USA.* 2000; 97:2264–2269. [PubMed: 10681455]
- [49]. Nishino A, Suzuki M, Ohtani H, Motohashi O, Umezawa K, Nagura H, Yoshimoto T. *J. Neurotrauma.* 1993; 10:167–179. [PubMed: 7692071]
- [50]. Arai T, Miklossy J, Klegeris A, Guo J-P, McGeer PL. *J. Neuropathol. Exp. Neurol.* 2006; 65:19–25. [PubMed: 16410745]
- [51]. Cho EJ, Lee J-W, Ellington AD. *Annu. Rev. Anal. Chem.* 2009; 2:241–264.
- [52]. Keefe AD, Pai S, Ellington A. *Nat. Rev. Drug. Discov.* 2010; 9:537–550. [PubMed: 20592747]
- [53]. Bock LC, Griffin LC, Latham JA, Vermaas EH, Toole JJ. *Nature.* 1992; 355:564–566. [PubMed: 1741036]
- [54]. Padmanabhan K, Padmanabhan KP, Ferrara JD, Sadler JE, Tulinsky A. *J. Biol. Chem.* 1993; 268:17651–17654. [PubMed: 8102368]
- [55]. Buff MCR, Schäfer F, Wulffen B, Müller J, Pöttsch B, Heckel A, Mayer G. *Nucleic Acids Res.* 2010; 38:2111–2118. [PubMed: 20007153]
- [56]. Ho H-A, Leclerc M. *J. Am. Chem. Soc.* 2004; 126:1384–1387. [PubMed: 14759196]
- [57]. Li N, Ho C-M. *J. Am. Chem. Soc.* 2008; 130:2380–2381. [PubMed: 18247609]
- [58]. Zhou W-J, Halpern AR, Seefeld TH, Corn RM. *Anal. Chem.* 2011; 84:440–445. [PubMed: 22126812]
- [59]. Xiao Y, Lubin AA, Heeger AJ, Plaxco KW. *Angew. Chem. Int. Ed.* 2005; 44:5456–5459.
- [60]. Radi A-E, Sánchez J. L. Acero, Baldrich E, O’Sullivan CK. *J. Am. Chem. Soc.* 2005; 128:117–124. [PubMed: 16390138]
- [61]. Lin Z, Chen L, Zhu X, Qiu B, Chen G. *Chem. Commun.* 2010; 46:5563–5565.
- [62]. Lin P-H, Chen R-H, Lee C-H, Chang Y, Chen C-S, Chen W-Y. *Colloids Surf., B.* 2011; 88:552–558.
- [63]. Wolf LK, Gao Y, Georgiadis RM. *J. Am. Chem. Soc.* 2007; 129:10503–10511. [PubMed: 17685519]
- [64]. Chen Y, Nakamoto K, Niwa O, Corn RM. *Langmuir.* 2012; 28:8281–8285. [PubMed: 22458258]

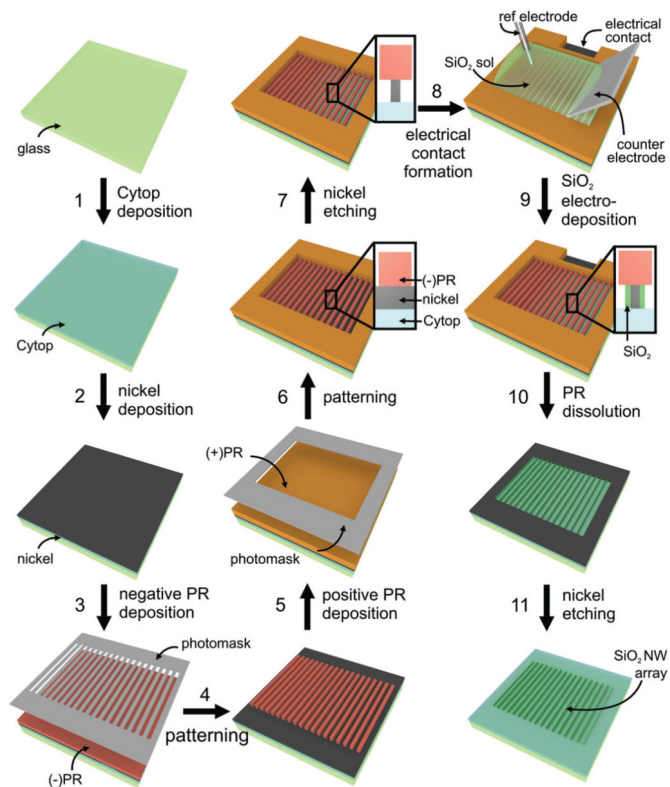


Figure 1. Schematic of the process used for the fabrication of SiO₂ NWs arrays.

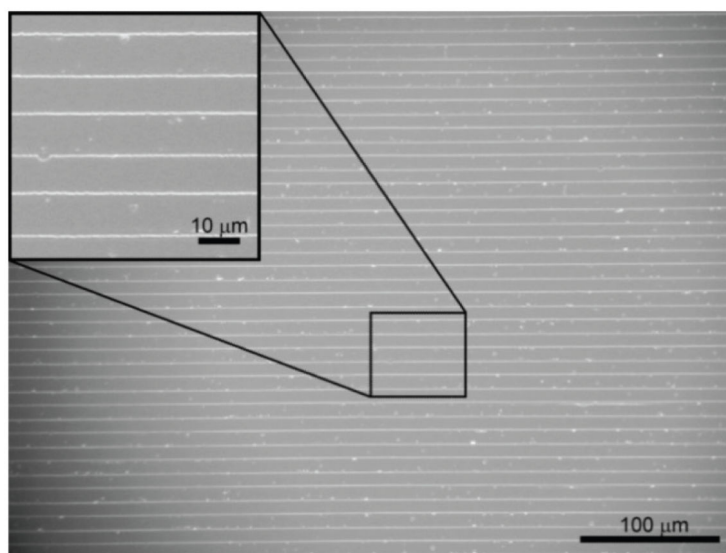


Figure 2. Optical micrograph showing a silica nanowire array. Inset: magnification of the squared area.

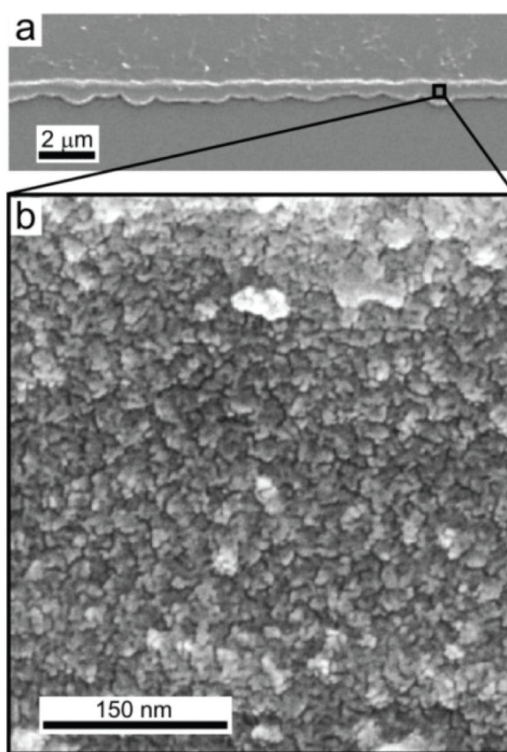


Figure 3.
a) SEM picture of a section of a single silica nanowire. b) High magnification SEM picture showing the surface of a silica nanowire.

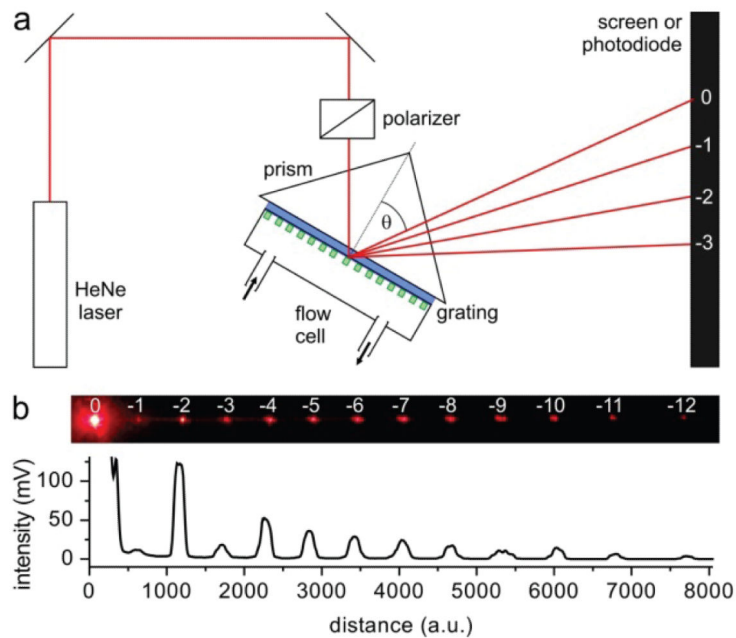


Figure 4.

a) Scheme showing the set-up used for the analysis of the silica nanowire grating diffraction using TIR geometry. b) Top: photograph of the diffraction pattern of a silica nanowire array taken in water. Bottom: corresponding intensity profile of the diffraction pattern.

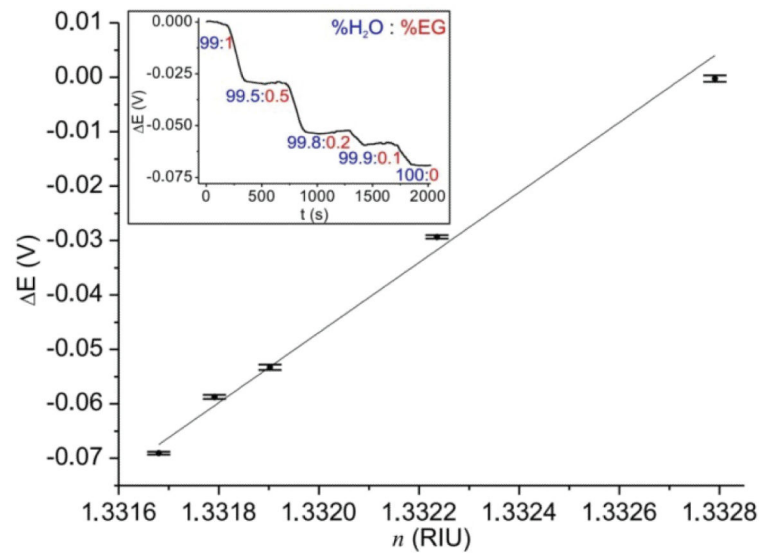


Figure 5. Plot of the difference of photodiode potential ΔE as a function of the refractive index of the solution injected in the flow cell n . Inset: detection curve showing the difference of photodiode potential as a function of time with different mixtures of water and ethylene glycol injected in the flow cell.

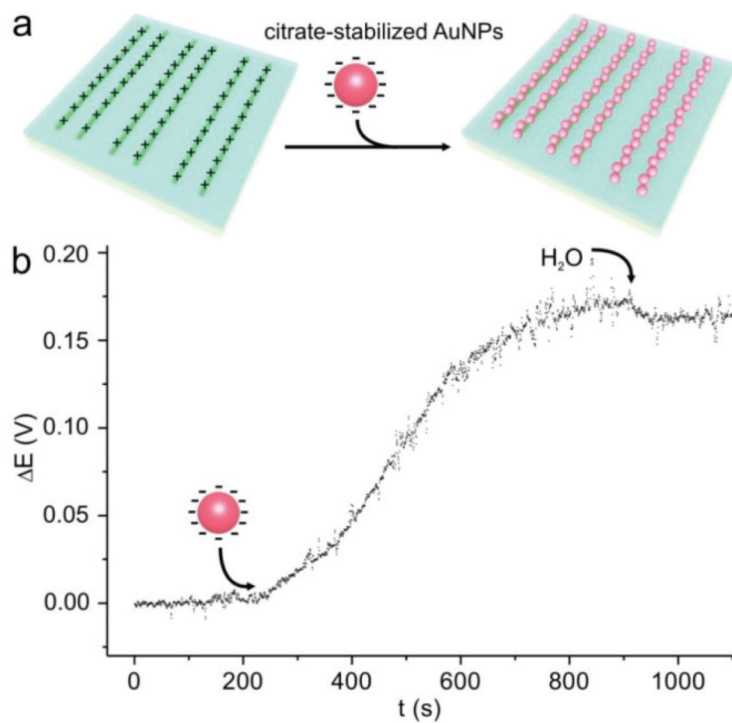


Figure 6.

a) Scheme showing the *in situ* electrostatic adsorption of negatively-charged gold nanoparticles on positively-charged silica nanowires. b) Curve of the difference of photodiode potential as a function of the time showing the electrostatic adsorption of gold nanoparticles on silica nanowires.

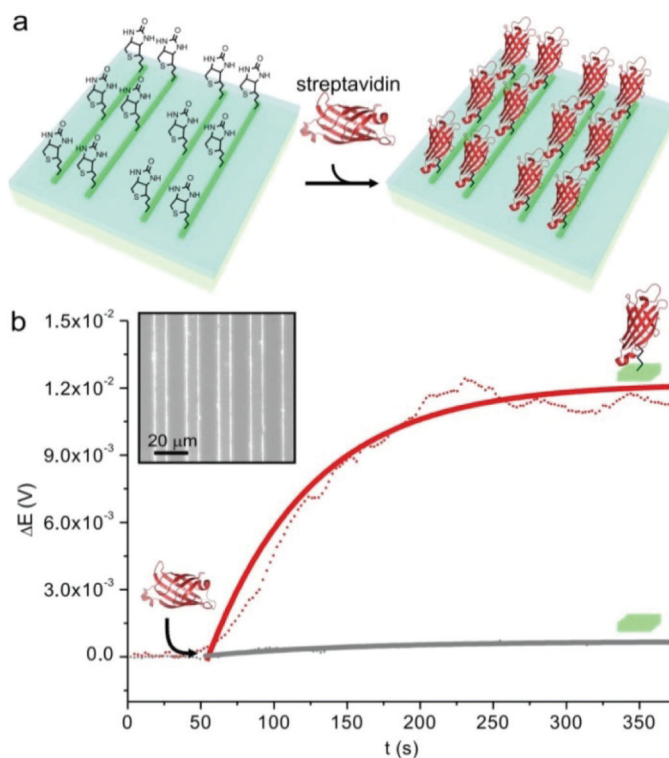


Figure 7.

a) Scheme showing the attachment of streptavidin on biotin-functionalized silica nanowires.

b) Binding curves of the interaction of streptavidin with biotin-functionalized silica nanowires (red) and with non-functionalized silica nanowires (grey). Dotted lines are the difference of photodiode potentials and solid lines are the fits of the difference of photodiode potentials with kinetic equation (3). Inset: Fluorescence microscopy image of silica nanowires functionalized with Alexa647-tagged streptavidin.

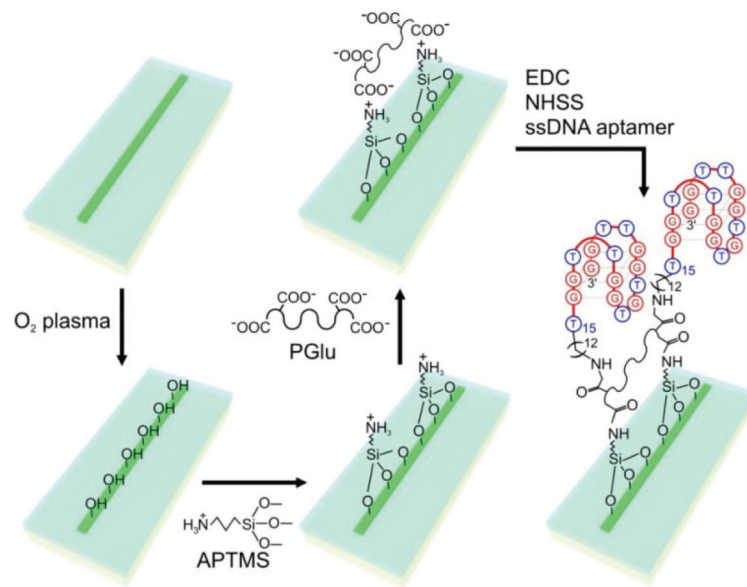
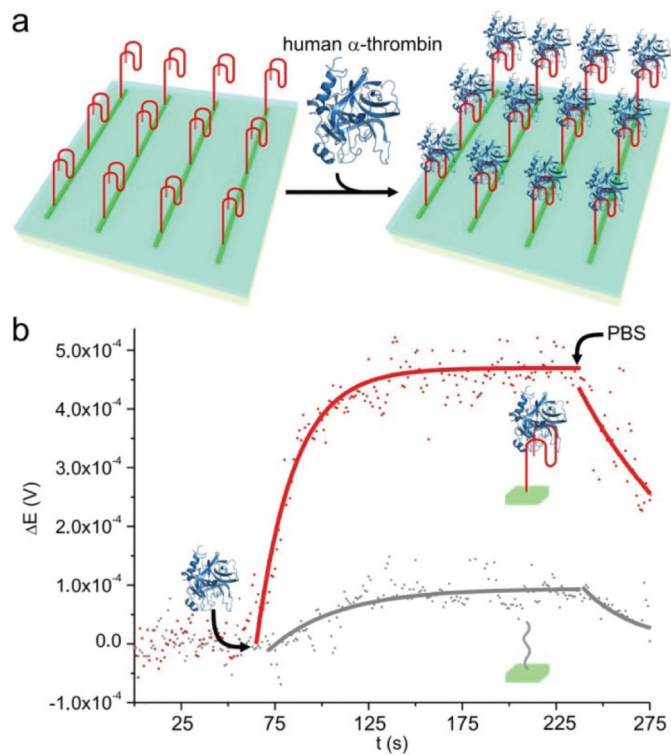


Figure 8. Scheme showing the functionalization of a silica nanowire with the thrombin binding ssDNA aptamer.

**Figure 9.**

a) Scheme showing the binding of human α -thrombin on aptamer-functionalized silica nanowires. b) Binding curves of human α -thrombin on thrombin-binding aptamer-functionalized silica nanowires (red) and on T_{30} -functionalized silica nanowires (grey). Dotted lines are the photodiode potentials shifts and solid lines are fits of equation (3) for the adsorption and (4) for the desorption.